pH sensing through a single optical fibre using SERS and CMOS SPAD line arrays

Ehrlich, Katjana; Kufcsák, Andras; McAughtrie, Sarah; Fleming, Holly; Krstajic, Nikola; Campbell, Colin J

Published in:
Optics Express

DOI:
10.1364/OE.25.030976

Publication date:
2017

Research Article | Vol. 25, No. 25 | 11 Dec 2017 | OPTICS EXPRESS 30976
Optics EXPRESS

pH sensing through a single optical fibre using SERS and CMOS SPAD line arrays

K. EHRLICH,[1,2,*] A. KUFCSÁK,[3] S. MCAUGHTRIE,[2,4] H. FLEMING,[4] N. KRSTAJIC,[2,3] C. J. CAMPBELL,[4] R. K. HENDERSON,[3] K. DHALIWAL,[2] R. R. THOMSON,[1,2] AND M. G. TANNER[1,2,5]

[1]*Scottish Universities Physics Alliance (SUPA), Institute of Photonics and Quantum Science, Heriot-Watt University, Edinburgh EH14 4AS, UK*
[2]*EPSRC IRC Hub in Optical Molecular Sensing & Imaging, MRC Centre for Inflammation Research, Queen's Medical Research Institute, University of Edinburgh, 47 Little France Crescent, Edinburgh EH16 4TJ, UK*
[3]*Institute for Integrated Micro and Nano Systems, School of Engineering, University of Edinburgh, King's Buildings, Alexander Crum Brown Road, Edinburgh EH9 3FF, UK*
[4]*School of Chemistry, EaStChem, University of Edinburgh, Joseph Black Building, West Mains Road, Edinburgh EH9 3FF, UK*
[5]*M.Tanner@hw.ac.uk*
[*]*ke9@hw.ac.uk*

Abstract: Full exploitation of fibre Raman probes has been limited by the obstruction of weak Raman signals by background fluorescence of the sample and the intrinsic Raman signal of the delivery fibre. Here we utilised functionalised gold nanoshells (NS) to take advantage of the surface-enhanced Raman spectroscopy (SERS) effect to enhance the pH responsive spectrum of 4-mercaptobenzoic acid (MBA). However, the fibre background is still dominant. Using the photon arrival time-resolving capability of a CMOS single-photon avalanche diode (SPAD) based line sensor, we recover the SERS spectrum without a fibre background in a 10 s measurement. In this manner, pH sensing through a multimode fibre at a low excitation power that is safe for future *in vivo* applications, with short acquisition times (10 or 60 s), is demonstrated. A measurement precision of ± 0.07 pH units is thus achieved.

OCIS codes: (300.6500) Spectroscopy, time-resolved; (030.5260) Photon counting.

References and links

1. N. Stone, C. Kendall, J. Smith, P. Crow, and H. Barr, "Raman spectroscopy for identification of epithelial cancers," Faraday Discuss. **126**, 141–157, discussion 169–183 (2004).
2. P. Crow, B. Barrass, C. Kendall, M. Hart-Prieto, M. Wright, R. Persad, and N. Stone, "The use of Raman spectroscopy to differentiate between different prostatic adenocarcinoma cell lines," Br. J. Cancer **92**(12), 2166–2170 (2005).
3. C. A. Lieber, H. E. Nethercott, and M. H. Kabeer, "Cancer field effects in normal tissues revealed by Raman spectroscopy," Biomed. Opt. Express **1**(3), 975–982 (2010).
4. E. B. Hanlon, R. Manoharan, T.-W. Koo, K. E. Shafer, J. T. Motz, M. Fitzmaurice, J. R. Kramer, I. Itzkan, R. R. Dasari, and M. S. Feld, "Prospects for in vivo Raman spectroscopy," Phys. Med. Biol. **45**(2), R1–R59 (2000).
5. O. Stevens, I. E. Iping Petterson, J. C. C. Day, and N. Stone, "Developing fibre optic Raman probes for applications in clinical spectroscopy," Chem. Soc. Rev. **45**(7), 1919–1934 (2016).
6. M. G. Shim, B. C. Wilson, E. Marple, and M. Wach, "Study of Fiber-Optic Probes for in Vivo Medical Raman Spectroscopy," Appl. Spectrosc. **53**, 619–627 (1999).
7. D. Wei, S. Chen, and Q. Liu, "Review of Fluorescence Suppression Techniques in Raman Spectroscopy," Appl. Spectrosc. Rev. **50**, 387–406 (2015).
8. U. Utzinger and R. R. Richards-Kortum, "Fiber optic probes for biomedical optical spectroscopy," J. Biomed. Opt. **8**(1), 121–147 (2003).
9. J. C. C. Day and N. Stone, "A Subcutaneous Raman Needle Probe," Appl. Spectrosc. **67**(3), 349–354 (2013).
10. D. Choudhury, M. G. Tanner, S. McAughtrie, F. Yu, B. Mills, T. R. Choudhary, S. Seth, T. H. Craven, J. M. Stone, I. K. Mati, C. J. Campbell, M. Bradley, C. K. I. Williams, K. Dhaliwal, T. A. Birks, and R. R. Thomson, "Endoscopic sensing of alveolar pH," Biomed. Opt. Express **8**(1), 243–259 (2016).

#307131 https://doi.org/10.1364/OE.25.030976
Journal © 2017 Received 14 Sep 2017; revised 27 Oct 2017; accepted 30 Oct 2017; published 27 Nov 2017

Optics EXPRESS

11. I. Gusachenko, M. Chen, and K. Dholakia, "Raman imaging through a single multimode fibre," Opt. Express **25**(12), 13782–13798 (2017).
12. W. Becker, *Advanced Time-Correlated Single Photon Counting Techniques* (Springer Berlin Heidelberg, 2005).
13. A. Campion and P. Kambhampati, "Surface-enhanced Raman scattering," Chem. Soc. Rev. **27**, 241 (1998).
14. P. R. Stoddart and D. J. White, "Optical fibre SERS sensors," Anal. Bioanal. Chem. **394**(7), 1761–1774 (2009).
15. S. W. Bishnoi, C. J. Rozell, C. S. Levin, M. K. Gheith, B. R. Johnson, D. H. Johnson, and N. J. Halas, "All-optical nanoscale pH meter," Nano Lett. **6**(8), 1687–1692 (2006).
16. T. Rojalin, L. Kurki, T. Laaksonen, T. Viitala, J. Kostamovaara, K. C. Gordon, L. Galvis, S. Wachsmann-Hogiu, C. J. Strachan, and M. Yliperttula, "Fluorescence-suppressed time-resolved Raman spectroscopy of pharmaceuticals using complementary metal-oxide semiconductor (CMOS) single-photon avalanche diode (SPAD) detector," Anal. Bioanal. Chem. **408**(3), 761–774 (2016).
17. J. Kostamovaara, J. Tenhunen, M. Kögler, I. Nissinen, J. Nissinen, and P. Keränen, "Fluorescence suppression in Raman spectroscopy using a time-gated CMOS SPAD," Opt. Express **21**(25), 31632–31645 (2013).
18. I. Nissinen, J. Nissinen, P. Keränen, A. K. Länsman, J. Holma, and J. Kostamovaara, "A Multitime-Gated SPAD Line Detector for Pulsed Raman Spectroscopy," IEEE Sens. J. **15**, 1358–1365 (2015).
19. C. Zhang, L. Zhang, R. Yang, K. Liang, and D. Han, "Time-Correlated Raman and Fluorescence Spectroscopy Based on a Silicon Photomultiplier and Time-Correlated Single Photon Counting Technique," Appl. Spectrosc. **67**(2), 136–140 (2013).
20. K. Ehrlich, A. Kufcsák, N. Krstajić, R. K. Henderson, R. R. Thomson, and M. G. Tanner, "Fibre optic time-resolved spectroscopy using CMOS-SPAD arrays," Proc. SPIE **10058**, 100580H (2017).
21. E. A. G. Webster, L. A. Grant, and R. K. Henderson, "A High-Performance Single-Photon Avalanche Diode in 130-nm CMOS Imaging Technology," IEEE Electron Device Lett. **33**, 1589–1591 (2012).
22. N. Krstajić, J. Levitt, S. Poland, S. Ameer-Beg, and R. Henderson, "256 × 2 SPAD line sensor for time resolved fluorescence spectroscopy," Opt. Express **23**(5), 5653–5669 (2015).
23. A. Kufcsák, A. Erdogan, R. Walker, K. Ehrlich, M. Tanner, A. Megia-Fernandez, E. Scholefield, P. Emanuel, K. Dhaliwal, M. Bradley, R. K. Henderson, and N. Krstajić, "Time-resolved spectroscopy at 19,000 lines per second using a CMOS SPAD line array enables advanced biophotonics applications," Opt. Express **25**(10), 11103–11123 (2017).
24. A. T. Erdogan, R. Walker, N. Finlayson, N. Krstajic, G. O. S. Williams, and R. K. Henderson, "A 16.5 giga events/s 1024 x 8 SPAD line sensor with per-pixel zoomable 50ps-6.4ns/bin histogramming TDC," in *2017 Symposium on VLSI Circuits* (2017), pp. C292–C293.
25. P. Matousek, M. Towrie, C. Ma, W. M. Kwok, D. Phillips, W. T. Toner, and A. W. Parker, "Fluorescence suppression in resonance Raman spectroscopy using a high-performance picosecond Kerr gate," J. Raman Spectrosc. **32**, 983–988 (2001).
26. J. Holma, I. Nissinen, J. Nissinen, and J. Kostamovaara, "Characterization of the Timing Homogeneity in a CMOS SPAD Array Designed for Time-Gated Raman Spectroscopy," IEEE Trans. Instrum. Meas. **66**, 1837–1844 (2017).
27. S. A. Grant and R. S. Glass, "Sol-gel-based biosensor for use in stroke treatment," IEEE Trans. Biomed. Eng. **46**(10), 1207–1211 (1999).

1. Introduction

Raman spectroscopy, based on exploiting the inelastic scattering of light from a sample, is often used for histochemical analysis such as discrimination of malignant and benign tissue [1–3]. The advantages for *in vivo* investigations are that it is non-destructive and minimally invasive, exhibits high spatial resolution, is chemically sensitive and has a rapid response which is important for *in situ* diagnosis [4]. However, the small cross section of the Raman scattering results in a weak signal, especially when exciting in the near-infrared regime ($1/\lambda^4$-dependency). The signal is often further obscured by fluorescence from surrounding regions e.g. tissue in medical applications. Additionally, *in vivo* measurements require optical fibre probes to reach the position of interest in the body. The optical fibre exhibits a high Raman scattering from the core material which contrary to other fluorescence background, is constant and scales with the fibre length itself [5,6]. This combination of unwanted background signals makes *in vivo* Raman spectroscopy extremely challenging, especially with a miniaturized fibre probe.

Efforts in recent years in response to the challenge have included methods of fluorescent background suppression [7]. However, while some are not applicable for *in vivo* applications, others suffer from sophisticated and expensive set-ups or long acquisition times. Meanwhile several commercial and non-commercial fibre Raman probes have been developed with methods for background suppression ranging from advanced fibre designs [8–10] to complex correction methods [11].

Optics EXPRESS

We demonstrate a time-correlated single photon counting (TCSPC) [12] spectrometry technique in combination with surface-enhanced Raman spectroscopy (SERS) [13] to overcome the challenges and enable a background free Raman spectrum with an ultra-miniaturised single fibre probe. The size and simplicity (moving the advanced and costly apparatus outside the fibre probe) enables endoscopic application in size restricted regions (e.g. the distal lung) with a disposable sensing probe. We exemplify the system for pH sensing with 4-mercaptobenzoic acid (MBA). pH is a key marker for the acid-base balance in metabolism which is tightly regulated but can be locally changed by pathologies such as inflammation and cancer. As an example, generation of an acidic environment increases growth of bacteria and inhibits antibiotics [10]. Quantifying and monitoring the environmental pH *in vivo* as enabled by this work has potential to improve diagnostics and therapy.

In this paper, we produce a sensing probe through the deposition of MBA functionalised gold nanoshells (NS) on the tip of the delivery fibre optic [10,14]. The gold NS have been designed as optical nanosensors for localized measurements of pH *in vivo*. They are robust, designed for use in the near-infrared spectral region, avoiding distortion from excessive autofluorescence from tissue and blood, and exhibit a continuous signal over a wide range of pH [15].

We remove fluorescent and fibre backgrounds through post-processing time-gating using the TCSPC capabilities of a complementary metal-oxide semiconductor (CMOS) single-photon avalanche diode (SPAD) based line sensor. We exploit the different time profiles of background fluorescence, fibre Raman scattering and the SERS signal to separate signal from background [16–19].

The TCSPC capable CMOS SPAD line sensor detects single photons and generates histograms according to their arrival time for 256 pixels simultaneously which are correlated to different wavelengths [20]. The advantages are high efficiency [21] and high time resolution (< 500 ps time stamping resolution) to record luminescent kinetics down to the nanosecond regime. This enables the utilisation of low excitation power (< 1 mW) and short exposure times (10 s - 60 s) thus enabling further development towards the *in vivo* sensing of physiological parameters. The technique is only limited by photon statistic constraints known as counting loss and pile-up, and inherent limitations on the performance of the SPADs; detector dead-time, dark count rate, varying photon detection probabilities, crosstalk and afterpulsing [12]. The exploitation of this advanced measurement system enables suppression of the unwanted background in the fibre-based Raman probe, facilitating the recovery of the background free spectrum. We demonstrate how this enables low power, rapid pH sensing through a multi-mode fibre with functionalised gold NS achieving improved measurement precision.

2. Material and methods

2.1. Optical setup

The measurements were performed using the time-resolved spectrometer shown schematically in Fig. 1. It consists of four parts: i) The excitation source was a 785 nm pulsed laser (LDH-D-F-N-780 and PDL 800-D, PicoQuant, spectral FWHM < 0.35 nm). The laser when operated at maximum power has a short leading pulse with a FWHM of 30 ps as stated in the manual specific to this laser, however it exhibits a long tail with a FWHM of 1.5 ns containing ¾ of the power. The average power was reduced with neutral density filters to 0.8 mW, this is safe for *in vivo* measurement and below the damage threshold for the sensors in continuous operation. The repetition rate was 20 MHz, as such, a full measurement of light transiting the length of a 2.7 m fibre and being backscattered to the detector was completed before the next laser pulse. ii) An optical coupling and collection system which was based on the same arrangement as standard for epi-fluorescence measurement. iii) A spectrometer based on a collimation lens, f = 50 mm, a transmission grating (1624 grooves / mm, Wasatch)

Optics EXPRESS

and a focusing lens, f = 30 mm (both Achromat Doublets, Thorlabs), ensuring a spectral range of 80 nm across the line array centred at 870 nm and a throughput of 78%, measured with a photodiode (S120C Thorlabs). iv) The in-house made CMOS SPAD sensor consisted of 256 pixels in a single line manufactured with 130 nm CMOS technology. The sensor timestamps the single photon events internally and simultaneously for all pixels. For further information about this sensor see [22,23]. This and the lack of any scanning element [16,17], for scanning along the spectral or temporal axis, ensures short measurement times. The dispersion was 0.3 nm/pixel and the spectral resolution was 1.6 nm or 25 cm^{-1}, limited by entrance slit width, grating density and lens combination. The temporal resolution set by the time-to-digital converter (TDC) was 423 ± 3 ps. The signal level was kept low to ensure a detector count rate of < 1% of the laser excitation rate and < 50% of the detector readout frame rate. The fibre-coupled design is extremely versatile and flexible for a broad range of applications and with the potential to be compact and mobile, suitable for *in situ* applications.

Two lengths of delivery optical fibres were used to act as passive fibre sensors with functionalised gold NS deposit at the fibre tip: a 2.7 m and an 18 m multimode fibre (both FG050LGA, Thorlabs). The protocol for the SERS preparation can be found in Section A.2.

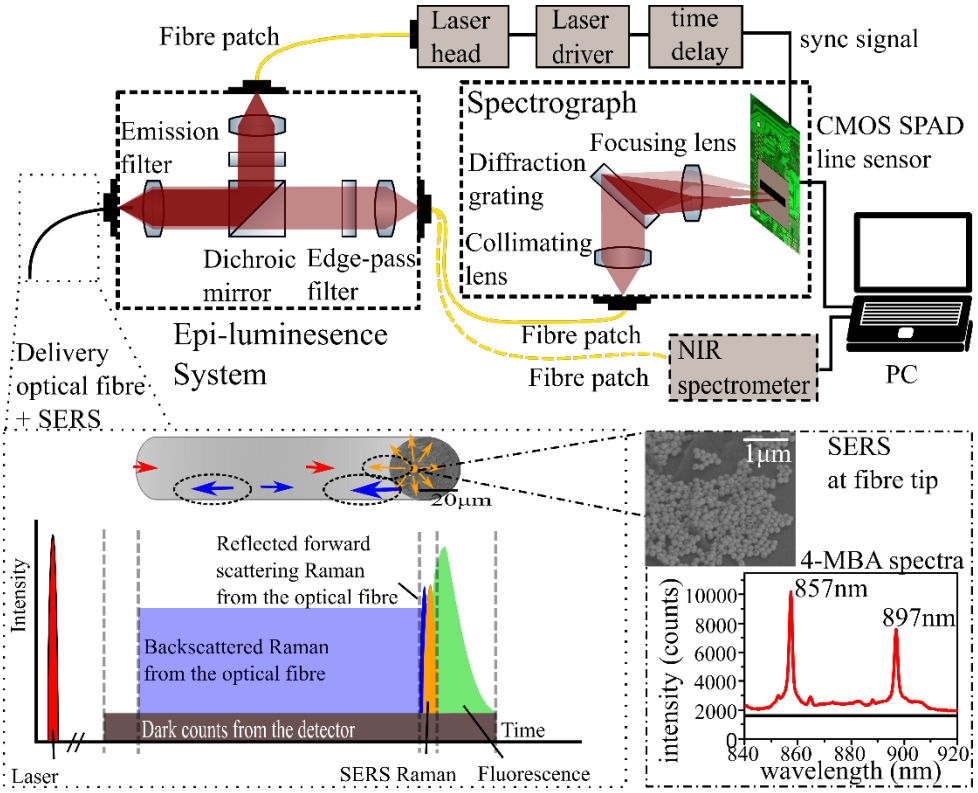

Fig. 1. A schematic of the time-resolved spectrometer and the principles of time-resolved measurements through an optical fibre with gold NS deposited on the fibre tip. The fibre tip of the multimode optical fibre (NA 0.22, 50 µm, Thorlabs) is covered with functionalised gold NS (150 nm, Bare Auroshell), as shown in the SEM image. The free-space spectrum of the functionalised MBA molecule taken with a Raman Probe and a QEPro spectrometer (OceanOptics). The integration time is 10 s and excitation power is 0.8 mW comparable to the experimental settings later. The schematic of the evolution of the signals in time is not to scale, the separation bars are guidance for the eye.

Optics EXPRESS

2.2 Data analysis

Utilizing the experimental setup and procedure outlined, a single measurement yields a 2-dimensional data array consisting of the spectral axis, the temporal axis and intensity data in terms of number of counts per pixel and per time bin. For gathering the spectral information, each pixel is correlated to a certain wavelength range. The temporal information is gained by measuring the arrival time of the photons and histogramming them for each pixel with the on-chip TCSPC functionality of the sensor.

"Noisy pixels" exhibit excessively high dark count rates due to fabrication variations and being electronically closer to their avalanche condition. The data of these pixels are removed from the measurement to avoid introducing excessive noise in the result. An average of 26% of the 256 pixels are identified as 'noisy pixels' through two identification methods: i) For a homogenous background (e.g. in Fig. 2(b) where there is a region of only dark counts), the average dark count level is taken as a threshold and the data of all pixels above this threshold are removed. ii) For a non-homogenous background, for example with an underlying signal (e.g. if the time of travel through the fibre or a fluorescent decay exceeds the measurement period as discussed later), a moving average method is used. The moving average is calculated over a window size of 5 adjacent pixels. If the data of one pixel is greater than the average plus the standard deviation of this subset, it is removed.

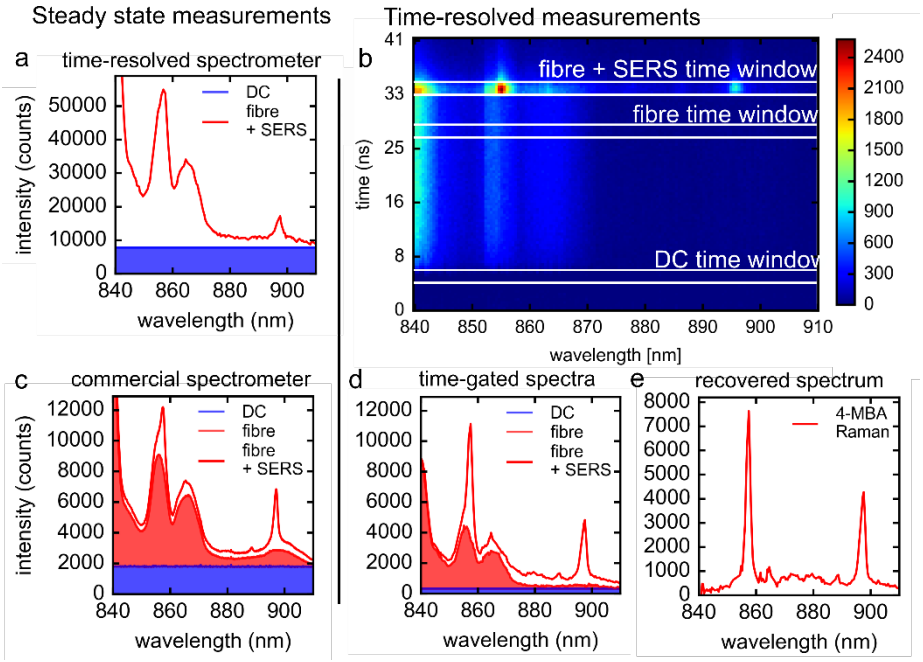

Fig. 2. 10 s measurement of a 2.7 m multimode optical fibre with functionalised gold NS at the fibre tip. (a) Non time-resolved measurement of the time-resolved spectrometer. (b) A 3-dimensional representation of the time-resolved measurement. Noisy pixels are removed and dark counts are subtracted. (c) Non time-resolved measurement with a commercial spectrometer (QEPro, Ocean Optics). (d) Time-gated spectra originating from the time windows indicated in (b). Time window width is 5 time bins or 2.1 ns. (e) A recovered spectrum from the MBA molecule.

As seen in Figs. 2(b) and 2(d), a full data analysis from one measurement is enabled by slicing the data into three time windows along the histogram axis. The average background count level per pixel is derived from the dark count 'DC' time window shown in Fig. 2(b) and subtracted pixel-wise as detector pixels exhibit differing count rates. Note that in the case of a signal that exceeds the duration of the measurement period determined by the repetition rate,

Optics EXPRESS

this time window contains not only detector background but also any other background signal such as fibre Raman or long lived fluorescence. The photon shot noise from these counts is still present in the final data. The 'fibre' time window contains the information about the backscattered fibre Raman spectral shape which can be used with a scaling factor to subtract the remaining fibre Raman signal from the 'fibre + SERS' time window (largely from the forward scattered fibre Raman) and thus the spectral information of MBA (as seen in Fig. 2(e)) can be recovered without a fibre background. Because of the uniformity of the fibre Raman, the time window can be placed anywhere along the fibre Raman signal. The scaling factor is needed to account for the reflection of the forward scattered fibre Raman on the multiple surfaces (fibre, NS, sol-gel).

3. Results and discussions

3.1 Enhanced visibility of the Raman signal through post-processing time-gating

Figure 2(a) and 2(c) demonstrate that the time-resolved spectrometer, without applying the time windows, offers visually similar spectra to the commercial spectrometer with some important differences. The time-resolved spectrometer has a higher efficiency (producing larger overall signal amplitudes) but a lower spectral resolution leading to broadening and lower peak visibility for the SERS features at ~860 nm and ~900 nm compared to the commercial spectrometer. Meanwhile, the ratio of detector dark counts to signal is comparable between the reference measurement and the time-resolved spectrometer measurement (as shown in Figs. 2(a) and 2(c)). Through post-processing time-gating, the detector dark counts and the unwanted fibre Raman can be significantly suppressed and the visibility of the SERS Raman signal can be significantly increased (see Fig. 2(d)). For clearer observation of the Raman spectra, the measured fibre background (from the 'fibre' time window) is subtracted, demonstrating clear recovery of the true spectra from the fibre tip (see Fig. 2(e)).

When time-gating the data the background counts are clearly reduced, thus reducing the background photon shot noise. For the purpose of this paper, we choose a time window of 5 time bins. This maximizes the signal-to-background (S/B) by removing the majority of the fibre background while additionally collecting the desired Raman signal over multiple time bins. However, increasing the time window width further than 5 time bins decreases S/B (see Appendix A.1.). For a fibre Raman dominant background, the S/B obtained was 4 × better in the time-gated result than that measured with the commercial spectrometer (integrated over the 857 nm peak). For a dark count dominated background, the S/B was 19 × better in the time-gated result than with the commercial spectrometer (897 nm peak), see Figs. 2(c) and 2(d).

These results could be improved if the instrument response function of the detector [23,24] and the pulse width of the laser were shorter (as discussed in Appendix A.1.), since the laser exhibits a long tail when operated at high power. The time-gating method in this paper is achieved by recording a whole TCSPC measurement and applying time windows to the data during post-processing. Others have presented time domain gating techniques such as streak cameras, electronically time-gated CCDs or CMOS detectors and optical driven Kerr gates [25]. While the latter achieves a time resolution of picoseconds, the setup is costly and measurement times lengthy (min). Electronic time-gating introduces additional jitter to the measurement through the enabling and disabling of the detector but potentially decreases the measurement time. However, we believe that time-gating in single photon counting (SPC) modality has no time advantage over TCSPC measurements in low light scenarios such as expected for *in vivo* sensing as measurement rate is limited by photon budget, not detector readout.

In biological applications, measurement of the SERS signal can be complicated further by fluorescence from delivered fluorophores or tissue autofluorescence which is always present. Figures 3(a)-3(c) shows how applying the time windows reduces the influence of the

Optics EXPRESS

fluorescent background due to the differing time scales of Raman and fluorescence, demonstrating how the MBA spectrum can be successfully recovered. In Fig. 3(a) the spectrum is dominated by a large broad fluorescence response, successfully removed in Fig. 3(b), with a clear recovered spectrum in Fig. 3(c). For other applications, such as remote environmental sensing, longer fibre lengths are useful. In TCSPC methodology, the laser repetition rate determines the temporal duration of the measurement. The time of travel for the photons through the optical fibre can be calculated with t = (2nL)/c, where L is the fibre length, n is the refractive index of the fibre core material and c the speed of light in vacuum. Modal dispersion in multimode fibres can be expected to be in the order of tens of picoseconds per metre. We collect signal in a 2.1 ns time window, as such broadening through modal dispersion does not contribute to our measurements of 3 m or 18 m fibres, but if longer multimode fibres were used it would affect the S/B and a longer time window width would be required. If the repetition rate is shorter than the time of travel, photons are counted against the following sync signal and the measurement seems to be 'wrapped around' the histogram axis. In Figs. 3(d)-3(f) an 18 m optical fibre with functionalised gold NS deposited at the fibre tip was measured within a 50 ns measurement period. The excitation power was reduced to 0.12 mW to ensure a single photon counting regime and the integration time was increased to 60 s. The fibre Raman signal is 'wrapped' around 3.6 times, increasing the unwanted background, before the SERS signal is seen in the histogram. This means photons are arriving from subsequent laser pulses in the same TDC bin, due to insufficient delay between pulses. The MBA spectrum can be recovered but suffers from higher shot noise and the use of the lower excitation power decreases the signal from the NS. However, it is clear that the SERS peaks not visible in Fig. 3(d) have been recovered in Fig. 3(f).

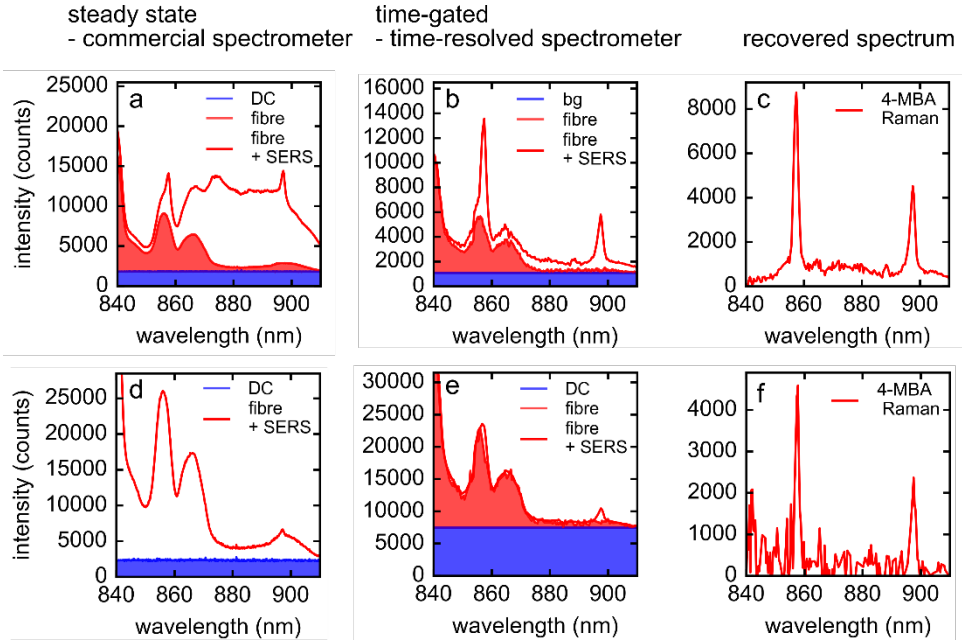

Fig. 3. (a)–(c) 10 s measurement of a 2.7 m multimode optical fibre with functionalised gold NS at the fibre tip and a high fluorescent background from a 3% phosphate Neodymium glass. (d)–(f) 60 s measurement of a 18 m multimode optical fibre with functionalised gold NS at the fibre tip. The excitation power is reduced to 0.12 mW. (a),(d) Reference measurement (QEPro, OceanOptics), (b),(e) time-gated measurement (5 time bins) (c),(f) recovered spectra of the MBA molecule.

As an alternate to the data in Figs. 3(d)-3(f), the same fibre can be measured with a 5 MHz repetition rate ensuring the time of travel does not exceed the measurement period or the

Optics EXPRESS

repetition rate of the laser. The expansion of the measurement period leads to a lower dark count level per time point (as DC are spread out over more time bins) but will increase the effect of the timing inhomogeneity of the CMOS SPADs [26], reducing the ability to accurately apply a narrow time window.

Additionally, to guarantee a single photon counting regime without pile-up [12], the average excitation power has to be decreased leading to both lower fibre Raman and SERS signal. If time is no constraint, a longer total measurement time compensates for the lower excitation power, and increases the accuracy of the measurement. However, for long fibres the combination of these factors results in a better recovered spectrum in the case of a short measurement period (high repetition rate) allowing the fibre background to wrap around, thus this method was chosen for the data shown here.

3.2. Application: pH sensing

The spectra of the MBA molecule is sensitive to environmental pH variations and has been previously demonstrated as a pH sensor [9, 21]. Ratiometric changes of the areas under the curve (AUC), within a 4.75 nm spectral window, around the peaks of 880 nm (1380 cm^{-1}) and 906 nm (1700 cm^{-1}) respectively, show the greatest pH sensitivity. Figure 4 shows that time-gating the data greatly increases the selectivity and reduces the standard deviation of the mean over 3 replicates in comparison to a non time-resolved measurement. Increasing the integration time from 10 s (as shown in Fig. 4(a)) to 60 s (as shown in Fig. 4(b)) increases the accuracy of the system further and hence the selectivity.

The precision of the time-resolved spectrometer was evaluated by obtaining the AUC ratios for pH 6 and 8 for 50 consecutively acquired measurements. For a 10 s measurement a repeatability of 0.14 and 0.19 pH units, for pH 6 and 8 respectively, was achieved with time-gating. For an integration time of 60 s this could be improved to 0.05 and 0.07 pH units, for pH 6 and 8 respectively. The precision of the pH sensor was determined by obtaining the AUC ratios while switching iteratively between pH 6 and 8 for 20 repeat measurements. For a 10 s measurement a repeatability of 0.25 and 0.30 pH units, for pH 6 and 8 respectively, was achieved with time-gating. Whilst, for an integration time of 60 s, this could be increased to 0.11 and 0.15 pH units, for pH 6 and 8 respectively.

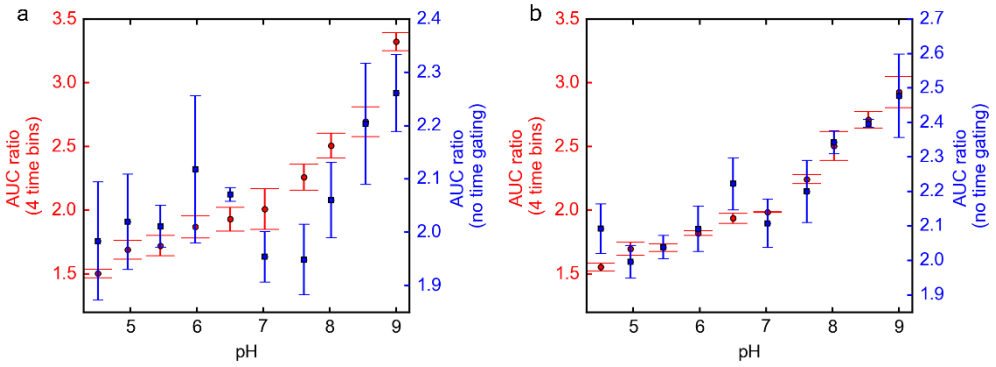

Fig. 4. Variation of area under the curve (AUC) ratio as a function of pH within the pH range of 4.5 to 9, the error bars represent the standard deviation of the mean over 3 replicate measurements. Each measurement was obtained using an average excitation power of 0.8 mW and 20 MHz pulse repetition rate, the integration was increased from a) 10 s to b) 60 s time-resolved measurement.

These results show that we are able to reach the same systematic stability which has been demonstrated earlier using the functionalised NS with a dual-core fibre and an adaptive iterative reweighted penalized least squares (airPLS) algorithm [10]. Decreased precision observed when switching between pH suggests some instability in the SERS sensors when

Optics EXPRESS

moving repeatedly over large pH changes. The observed limits in measurement repeatability are larger than those expected from counting statistics after post-processing time-gating, and are instead believed to be due to detector fluctuation (varying pixel dark counts and photon detection probabilities), bias voltage fluctuations or thermal instabilities. Active temperature stabilisation as applied to commercial detectors could offer improved results. We also believe that cooling would greatly reduce the dark counts of the detector, reducing the shot noise and leading to better stability and accuracy. Improved timing accuracy and laser pulse width would offer further improved S/B.

4. Conclusion

A time-resolved system for recovering the spectra of weak Raman signals without fibre or fluorescent backgrounds has been demonstrated. pH sensing through a single core multimode optical fibre using short measurement times was achieved as an example of application. This methodology has high potential for ultra-miniaturized Raman probes for *in vivo* endoscopic sensing of physiological parameters such as pH, oxygen or glucose concentration as well as for remote environmental sensing. In terms of accuracy, the limit of the line sensor was reached and improvement has to include further detector calibrations such as photon-detection variations and reduction of the dark counts through cooling. As time is crucial for *in situ* diagnosis scenarios, the already short integration time can be reduced further through on-chip time-gating capabilities which has been demonstrated with this specific CMOS SPAD line sensor elsewhere [23].

Appendix

A. 1. Signal-to-background investigation

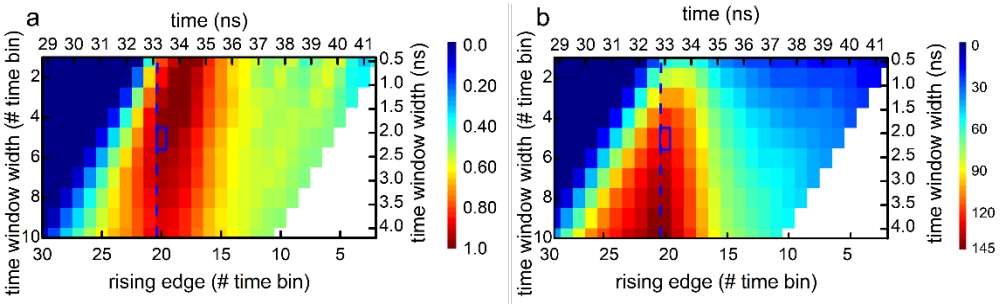

Fig. 5. (a) S/B and (b) S/N plotted against the rising edge of the time window and the width of the time window for the area under the 857 nm SERS peak. The blue vertical dashed line is shown to label the time onset of the signal from the end of the fibre. The blue box shows the chosen timing of bins selected for the other plots in this paper.

The S/B quantifies the 'visibility' of the Raman photons in comparison to the unwanted background photons, which includes the detector dark counts and fibre background. The signal-to-noise (S/N) is a measure for the noise present in the measurement of Raman photons within the whole signal.

$$\frac{S}{B} = \frac{N_R}{N_F + N_{DC}} \; and \; \frac{S}{N} = \frac{N_R}{\left(N_R + N_F + N_{DC}\right)^{1/2}} \tag{1}$$

where N_R is the integrated number of counts in the area under the SERS peak at 857 nm, N_F and N_{DC} are the integrated number of counts in the same area of the Raman scattering of the fibre and the detector noise, respectively. The area under the peak was chosen as representative of the Raman signal strength, allowing direct comparison between spectrographs of differing resolution.

Optics EXPRESS

While naively the shortest time window may seem to be optimum for improved signal to background or noise [17,26], this is not the case due to extended laser pulse and detector jitter. If the rising edge of the time window is kept constant at the onset of photon counts from the fibre tip, and the width of time window increased (as shown by following the line in Fig. 5) increased SERS signal photons are initially collected, due to the extended IRF of the measurement system, offering improved signal to background (as shown in Fig. 5(a)). However, as the time window is further increased, DC become more dominant than the decreasing tail of the SERS signal, and signal to background decreases. S/N follows a similar trend (see Fig. 5(b)), although a slightly longer time window gives optimum S/N due to the square root in Eq. (1)

Meanwhile, if the time window is misaligned to the SERS signal photon arrival (e.g. moving on the x axis of Fig. 5), or the window is increased in size in both directions around the SERS photon arrival (e.g. from a less accurate measurement system) both S/B and S/N are observed to rapidly decrease due to greater photon counts from the fibre Raman background being included in the data.

A time window of 5 bins was chosen as previously discussed for data in this paper, producing a compromise of good S/B and S/N. This can also be seen as marked visually as the 'fibre + SERS' time window in Fig. 2(b) to capture well the extent of the photons from the fibre tip. However, this once more indicates that a system (both laser and detector) with a shorter IRF would offer an improved measurement result as the time window could be reduced. In this work the limit was the laser pulse shape, extending for ~2 ns (from manufacturer specifications specific to our laser), matching to the optimal time-window determined analytically.

A.2. pH nanosensor preparation

Preparation of the functionalised NS: Gold NS (5 x 1 mL aliquots, $2x10^9$ particles/mL, ~ 150 nm, Bare AuroShell™ Particles in deionised water, Nanospectra Biosciences Inc.) were prepared for functionalisation by centrifugation at 5500 rpm for 10 min. Following centrifugation all or as much as possible of the supernatant was removed without disturbing the pellet. For functionalisation, the pellet was resuspended with distilled water (900 µL) and 4-MBA (100 µL, 1 mM in EtOH) and the samples were left overnight. The NS were washed to remove unbound molecule by centrifuging at 5500 rpm for 10 min. Following centrifugation all or as much as possible of the supernatant was removed without disturbing the pellet. The functionalised particles were then resuspended with 500 µL dH_2O and the samples were sonicated and vortexed to force the particles back into suspension. This washing procedure was repeated a total of 3×. Following washing the particle suspensions were centrifuged at 5500 rpm for 10 min and 450 µL of the supernatant was removed. The final volume remaining in each of the aliquots was measured by pipette and noted. Samples were again centrifuged at 5500 rpm for 10 min and the appropriate volume of supernatant was removed from each to leave a final volume of 5 µL. The individual aliquots (5 aliquots) were then combined to give a particle suspension with a final volume of 25 µL.

Loading of the fibre with functionalised NS: Binding of the functionalised NS and the fibre tip can be increased by enhancing their electrostatic interaction. To achieve this the fibre tip was soaked overnight in positively-charged poly-L-lysine (0.1 mg/mL in distilled water, 30000-70000 MW, Sigma Aldrich) The fibre tip was then removed from the poly-L-lysine solution and dried under nitrogen. The fibre tip was directly dipped into the functionalised NS suspension to coat the fibre. NS were added to the fibre tip until a maximized SERS Raman signal was observed. Currently, there is no control over the packaging density and distribution of the NS through this protocol (as seen in Fig. 1).

Sol-gel preparation for the fibre tip: After the NS had dried on to the fibre tip they were secured by dip coating a protective sol-gel. The sol-gel was prepared *via* the method set out

Optics EXPRESS

by Grant *et al.* [27] with MilliQ water being used instead of deionised water. The sol-gel was left to dry overnight.

Funding

UK Engineering and Physical Sciences Research Council (EPSRC, United Kingdom) Interdisciplinary Research Collaboration (EP/K03197X/1); Engineering and Physical Sciences Research Council and Medical Research Council (EP/L016559/1); James-Watt Scholarship from Heriot-Watt University.

Acknowledgments

We would like to further thank STMicroelectronics, Imaging Division, Edinburgh, for their support in manufacturing of the CMOS SPAD line sensors. The experimental data is available via Edinburgh DataShare (http://dx.doi.org/10.7488/ds/2241).